

## Accepted Manuscript

Adaptive least-squares finite element approximations to Stokes equations

Hsueh-Chen Lee, Tsu-Fen Chen

PII: S0377-0427(14)00520-2

DOI: <http://dx.doi.org/10.1016/j.cam.2014.11.041>

Reference: CAM 9884

To appear in: *Journal of Computational and Applied Mathematics*

Received date: 27 February 2013

Revised date: 17 October 2013

Please cite this article as: H.-C. Lee, T.-F. Chen, Adaptive least-squares finite element approximations to Stokes equations, *Journal of Computational and Applied Mathematics* (2014), <http://dx.doi.org/10.1016/j.cam.2014.11.041>

This is a PDF file of an unedited manuscript that has been accepted for publication. As a service to our customers we are providing this early version of the manuscript. The manuscript will undergo copyediting, typesetting, and review of the resulting proof before it is published in its final form. Please note that during the production process errors may be discovered which could affect the content, and all legal disclaimers that apply to the journal pertain.



# Adaptive Least-Squares Finite Element Approximations to Stokes Equations

Hsueh-Chen Lee<sup>a,1</sup>, Tsu-Fen Chen<sup>b,2</sup>

<sup>a</sup>General Education Center, Wenzao Ursuline University of Languages, Kaohsiung, Taiwan

<sup>b</sup>Department of Mathematics, National Chung Cheng University, Minghsiang, Chia-Yi, Taiwan

---

## Abstract

This paper is concerned with adaptive least-squares methods for Stokes equations based on velocity-pressure-stress and velocity-vorticity-pressure formulations. To capture the Stokes flow region, an adaptive algorithm based on mesh redistribution is developed for a nonlinear weighted least-squares functional. A redistribution approach is considered to generate the optimal grids. Model problems considered are the flow past a planar channel and a 4-to-1 contraction problems. Numerical results of model problems illustrating the efficiency of the proposed scheme are presented.

**Key words:** least-squares finite element, Stokes equation, nonlinear weighting function, mesh redistribution, adaptive graded mesh, grading function.

---

## 1. Introduction

In recent years, there has been much development of numerical algorithms to simulate flow problems. Although much progress has been made, there are some unresolved difficulties such as corner singularity, and the computational limitations arising from the presence of multiple dependent variables which requires a compatibility condition on the finite element spaces if the standard mixed methods approach are used, [1] and [2].

---

*Email addresses:* 87013@mail.wzu.edu.tw (Hsueh-Chen Lee),  
tfchen@math.ccu.edu.tw (Tsu-Fen Chen)

<sup>1</sup>Supported in part by the National Science Council of Taiwan under contract 100-2115-M-116-001.

<sup>2</sup>Corresponding author. Supported in part by the National Science Council of Taiwan under contract no. 100-2115-M-194-007.

*Preprint submitted to Journal of Computational and Applied Mathematics*

*October 17, 2013*

The least-squares finite element approach has been shown to offer several theoretical and computational advantages over Galerkin methods for a variety of boundary value problems, [3]. In particular, the algebraic system generated by the discretization is always symmetric and positive definite, there is no compatibility condition between finite element spaces for mixed methods, and the method is insensitive to equation type. The least-squares approximations of the incompressible Stokes equations based on both velocity-pressure-stress and velocity-vorticity-pressure formulations were considered in [3]. In [3], Bochev and Gunzburger presented a mesh-dependent least-squares finite element method. Based on these ideas, a nonlinear weighted least-squares finite element method (NWLS) was applied successfully to the Stokes equations using both formulations (see, [4] and [5]). In addition, using uniform meshes, results indicated that using linear approximations in all variables, the least-squares solutions exhibit optimal  $L^2$ -norm error convergence in all unknowns by choosing proper weighting functions. This approach is distinct from the class of methods known as Galerkin least-squares (GLS) in which least-squares terms are added to standard mixed formulations for stabilization. Examples of a GLS method applied to flow problem can be found in [6], [7], and [8].

Although promising results can be obtained using NWLS methods, one difficulty for solving the flow problems in the real case is the computational limitation arising from the exorbitant number of unknowns. To reduce the size of the linearized system of equations and resolve the singularity arising from the geometric discontinuity, adaptive grids aligned with the high gradient region are often necessary for more efficient and accurate results. In [9], two-point boundary value problems were considered by Carey and Dinh, and optimal grids were generated by equidistributing a grading function throughout the domain. The idea is to adjust the position of the grid points and produce a mesh with the same number of unknowns, which is more aptly graded for the given problem. Following Carey and Dinh's idea, based on finite element approximations, a mesh redistribution algorithm in two spatial dimensions was developed and applied to the convection dominated problems with great success [10]. Based on these ideas, adaptive least-squares finite element methods for viscoelastic flow problems were developed in [11]. In [11], results indicated that graded meshes agree with the physical attributes of these models and smoothed triangulation can improve convergence rates and errors. However, grid effects of nonuniform meshes were also reported in [11] for the NWLS method using lower-order basis functions.

The purpose of the paper is to present an effective adaptive nonlinear weighted

least-squares method for the Stokes equations using both velocity-pressure-stress and velocity-vorticity-pressure defined in [4] and [5], respectively. To capture the flow region, an adaptive algorithm based on the mesh redistribution with optimal graded mesh refinement is developed. In our computations, continuous piecewise linear finite element spaces for all variables are considered. For the planar flow problem, optimal  $L^2$ -norm error convergence in all variables are obtained for the adaptive least-squares using both formulations. Next, we extend the implementation to simulate the 4-to-1 contraction problem considered in [6]. In [6], Bonvin, et al. presented a reduced GLS method with equal order linear interpolation function that adds stabilized three-field formulations for the Stokes problem based on a linear version of the Oldroyd-B model. That paper also established the compatibility conditions for the approximation functions of the extra stress, velocity, and pressure fields. In this paper, we will show that the implementation of least-squares method is simpler and the results are compatible to those of the reduced GLS method presented in [6]. In addition, we will show that the grid effects reported in [11] of the NWLS method for the nonuniform meshes can be greatly reduced using the graded meshes constructed by the adaptive scheme.

This paper is organized as follows. In Section 2, governing equations for the Stokes equations of velocity-pressure-stress and velocity-vorticity-pressure formulations are introduced. Section 3 describes nonlinear weighted least-squares finite element formulations for both formulations. In Section 4, based on the derivation in Carey and Dinh [9], the grading function and numerical algorithm for Stokes flow problems are presented. Then, Section 5 provides the results of least-squares methods using both forms of the Stokes equations and grid effects will be studied using various grids. In addition, stability and optimal convergence of a hybrid adaptive grid based on the algorithm described in Section 4 will be illustrated. Finally, conclusions are drawn in Section 6.

## 2. Stokes equations

Consider the following generalized stationary Stokes problem in an open domain in  $\Omega = \mathbb{R}^d$ ,  $d = 2$  or  $3$  with boundary  $\Gamma$ :

$$\begin{aligned} -\eta\Delta\mathbf{u} + \nabla p &= \mathbf{f} \text{ in } \Omega, \\ \nabla \cdot \mathbf{u} &= 0 \text{ in } \Omega, \\ \mathbf{u} &= \mathbf{u}_0 \text{ on } \Gamma, \end{aligned} \tag{1}$$

where  $\mathbf{u}$  and  $p$  denote the velocity and pressure fields,  $\eta$  is a viscosity constant, and  $\mathbf{f}$  and  $\mathbf{u}_0$  are given functions. For uniqueness, we assume that the pressure  $p$

satisfies a zero mean constraint:

$$\int_{\Omega} p dx = 0.$$

Two first-order systems of the Stokes equations are considered here: the velocity-pressure-stress and velocity-vorticity-pressure. Let  $\mathbf{D}(\mathbf{u}) = \frac{1}{2} (\nabla \mathbf{u} + \nabla \mathbf{u}^T)$  denote the symmetric part of the velocity gradient. i.e., the deformation tensor. Defining the stress tensor  $\boldsymbol{\tau} := \sqrt{2\eta} \mathbf{D}(\mathbf{u})$  scaled by  $\sqrt{\eta/2}$ , we have the following generalized velocity-pressure-stress system (VPS) [3]:

$$\begin{aligned} \boldsymbol{\tau} - \sqrt{2\eta} \mathbf{D}(\mathbf{u}) &= \mathbf{f}_1 \text{ in } \Omega, \\ \nabla \cdot \mathbf{u} &= f_2 \text{ in } \Omega, \\ -\sqrt{2\eta} \nabla \cdot \boldsymbol{\tau} + \nabla p &= \mathbf{f}_3 \text{ in } \Omega, \\ \mathbf{u} &= \mathbf{u}_0 \text{ on } \Gamma. \end{aligned} \quad (2)$$

The velocity-vorticity-pressure formulation (VVP) of the Stokes problem, by the vorticity variable

$$\boldsymbol{\omega} := \nabla \times \mathbf{u},$$

can be cast into the first-order system [3]:

$$\begin{aligned} \nabla \times \mathbf{u} - \boldsymbol{\tau} &= \mathbf{f}_1 \text{ in } \Omega, \\ \nabla \cdot \mathbf{u} &= f_2 \text{ in } \Omega, \\ \eta \nabla \times \boldsymbol{\omega} + \nabla p &= \mathbf{f}_3 \text{ in } \Omega, \\ \mathbf{u} &= \mathbf{u}_0 \text{ on } \Gamma. \end{aligned} \quad (3)$$

In both systems (2) and (3), the function  $f_2$  satisfies the following solvability constraint:

$$\int_{\Omega} f_2 dx = \int_{\partial\Omega} \mathbf{u}_0 \cdot \mathbf{n} ds.$$

If the tensor  $\mathbf{f}_1$  and the function  $f_2$  are identically zero, the Stokes equations (1) are equivalent to both generalized systems (2) and (3). For simplicity, without loss of generality, we assume that  $\mathbf{u}_0 = 0$ .

Note that in two dimension, the curl of  $\mathbf{u}$  gives the scalar function

$$\nabla \times \mathbf{u} = \partial_1 u_2 - \partial_2 u_1,$$

where  $u_1$  and  $u_2$  are the components of  $\mathbf{u}$ . Therefore, the system (3) has four equations and four unknowns while the system (2) has six equations and six unknowns.

Since the system (3) involves fewer unknowns than does the stress formulation, it is more efficient to apply to the Navier-Stokes equation, [5]. As for the system (2), it was illustrated in [4] and [2] that the system is suitable for viscoelastic flows when a direct approximation of the extra stress tensor is desired.

The governing equations are solved on two domains: the first is a square test domain with exact boundary conditions and non-zero right-hand sides determined by the exact solution, which is used to measure convergence rates; the second domain is the 4-to-1 contraction, consisting of an upstream channel which abruptly narrows to a channel one quarter of the original width. The domains with boundaries labeled are shown in Figure 1 below. For the VPS and VVP formulations on

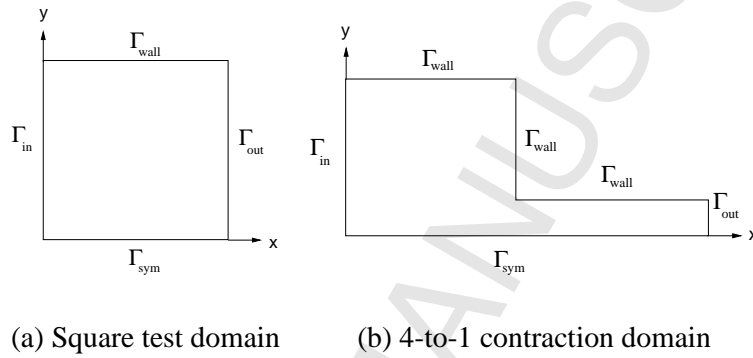


Figure 1: Computational domains

the test domain, the boundary conditions are as follows:

$$\mathbf{u} = \mathbf{u}_\Gamma \quad \text{on} \quad \Gamma_{in}, \Gamma_{wall}, \Gamma_{out}, \quad (4)$$

$$p = p_0 \quad \text{on} \quad \Gamma_{out} \cap \Gamma_{wall}, \quad (5)$$

$$\mathbf{u} \cdot \mathbf{n} = 0, \pi : \mathbf{nt} = 0 \quad \text{on} \quad \Gamma_{sym}, (\text{VPS only}) \quad (6)$$

$$\mathbf{u} \cdot \mathbf{n} = 0, \omega = 0 \quad \text{on} \quad \Gamma_{sym}, (\text{VVP only}). \quad (7)$$

For the VPS and VVP formulations on the 4-to-1 contraction domain, let  $\mathbf{u} =$

$(u, v)$ , and the boundary conditions are the following:

$$\mathbf{u} = \mathbf{u}_\Gamma \quad \text{on} \quad \Gamma_{in}, \quad (8)$$

$$\mathbf{u} = \mathbf{0} \quad \text{on} \quad \Gamma_{wall}, \quad (9)$$

$$v = 0, p = 0 \quad \text{on} \quad \Gamma_{out}, (\text{VPS only}) \quad (10)$$

$$v = 0, p = 0 \quad \text{on} \quad \Gamma_{out}, (\text{VVP only}) \quad (11)$$

$$\mathbf{u} \cdot \mathbf{n} = 0, \boldsymbol{\pi} : \mathbf{nt} = \mathbf{0} \quad \text{on} \quad \Gamma_{sym}, (\text{VPS only}) \quad (12)$$

$$\mathbf{u} \cdot \mathbf{n} = 0, \boldsymbol{\omega} = \mathbf{0} \quad \text{on} \quad \Gamma_{sym}, (\text{VVP only}), \quad (13)$$

where  $\mathbf{n}$  and  $\mathbf{t}$  are unit vectors outward normal and tangent to the boundary, respectively,  $\boldsymbol{\pi} = p\mathbf{I} - \boldsymbol{\tau}$  is the Cauchy stress tensor, and  $\mathbf{u}_\Gamma$  and  $\boldsymbol{\tau}_\Gamma$  are specified boundary functions. These boundary conditions are also used for the Stokes flow in [6].

### 3. Nonlinear weighted least-squares schemes

In this section, we present nonlinear weighted least-squares methods for VPS and VVP formulations of the Stokes equations. The function spaces used in our variational formulations are defined as:

$$\begin{aligned} \mathbf{V}^{square} &= \{ \mathbf{v} \mid \mathbf{v} \in [\mathbf{H}^1(\Omega)]^d, \mathbf{v} = \mathbf{u}_\Gamma \text{ on } \Gamma/\Gamma_{sym}, v_2 = (\mathbf{u}_\Gamma)_2 \text{ on } \Gamma_{sym} \} \\ \mathbf{V}^{4-to-1} &= \{ \mathbf{v} \mid \mathbf{v} \in [\mathbf{H}^1(\Omega)]^d, \mathbf{v} = \mathbf{u}_\Gamma \text{ on } \Gamma_{in}, \mathbf{v} = \mathbf{0} \text{ on } \Gamma_{wall}, v_2 = (\mathbf{u}_\Gamma)_2 \text{ on } \Gamma_{sym} \} \\ Q^{square} &= \{ q \mid q \in L^2(\Omega), q(x_0) = p_0 \text{ on } \Gamma_{out} \cap \Gamma_{wall} \} \\ Q^{4-to-1} &= \{ q \mid q \in L^2(\Omega), q = 0 \text{ on } \Gamma_{out} \} \\ \Sigma_s &= \{ \boldsymbol{\sigma} \mid \boldsymbol{\sigma} \in [L^2(\Omega)]^{2d}, \sigma_{ij} = \sigma_{ji} \} \\ \Sigma_v &= \{ \boldsymbol{\sigma} \mid \boldsymbol{\sigma} \in [L^2(\Omega)]^{2d-3} \}, \end{aligned}$$

where  $x_0$  and  $p_0$  are specified. Subsequent use of  $(\mathbf{V}, Q)$  for function spaces refers generically either to  $(\mathbf{V}^{square}, Q^{square})$  or  $(\mathbf{V}^{4-to-1}, Q^{4-to-1})$ . Also, the set of spaces for which homogeneous boundary conditions replace possibly nonzero Dirichlet boundary conditions in  $(\mathbf{V}, Q, \Sigma_s, \Sigma_v)$  is denoted  $(\mathbf{V}^0, Q^0, \Sigma_s^0, \Sigma_v^0)$ .

Now, we define the continuous piecewise polynomial finite element spaces. Let  $\Gamma_h$  be a family of regular partitions of the domain  $\Omega$ , specifically

$$\Gamma_h = \{ \Omega_k^h : k = 1, 2, \dots, N \}.$$

Here  $h = \frac{2\sqrt{A}}{\sqrt{N}}$ , where  $A$  is the area of the domain, and  $N$  is the number of triangular elements in the finite element discretization. Let  $P_r(\Omega_k^h)$  denote the space

of polynomials with degree less than or equal to  $r$  defined over  $\Omega_k^h$ . Define the following continuous piecewise polynomial finite element spaces:

$$\begin{aligned} V^h &= \{\mathbf{v}^h \mid \mathbf{v}^h \in \mathbf{V}, \mathbf{v}^h|_{\Omega_k^h} \in [P_r(\Omega_k^h)]^d, k = 1, 2, \dots, N\}, \\ Q^h &= \{q^h \mid q^h \in Q, q^h|_{\Omega_k^h} \in P_r(\Omega_k^h), k = 1, 2, \dots, N\}, \\ \Sigma_s^h &= \{\boldsymbol{\sigma}_s^h \mid \boldsymbol{\sigma}_s^h \in \Sigma_s, \boldsymbol{\sigma}_s^h|_{\Omega_k^h} \in [P_r(\Omega_k^h)]^{2d}, k = 1, 2, \dots, N\}, \\ \Sigma_v^h &= \{\boldsymbol{\sigma}_v^h \mid \boldsymbol{\sigma}_v^h \in \Sigma_v, \boldsymbol{\sigma}_v^h|_{\Omega_k^h} \in [P_r(\Omega_k^h)]^{2d-3}, k = 1, 2, \dots, N\}. \end{aligned}$$

The nonlinear weighted least-squares variational principle considered in [4] and [2] for the velocity-pressure-stress (VPS) formulation of system (2) is to find  $\mathbf{u} \in V^h$ ,  $p \in Q^h$ , and  $\boldsymbol{\tau} \in \Sigma_s^h$ , which minimize the functional

$$J_h(\mathbf{v}, q, \boldsymbol{\sigma}) = \left\| -\sqrt{2\eta} \nabla \cdot \boldsymbol{\sigma} + \nabla q \right\|_0^2 + Kh^{-2} \|\nabla \cdot \mathbf{v}\|_0^2 + h^{-2} \left\| w_s(\boldsymbol{\sigma} - \sqrt{2\eta} \mathbf{D}(\mathbf{v})) \right\|_0^2 \quad (14)$$

over all  $\mathbf{v} \in V^h$ ,  $q \in Q^h$ , and  $\boldsymbol{\sigma} \in \Sigma_s^h$ . Similarly, as in [5], the nonlinear weighted least-squares variational principle for the velocity-vorticity-pressure (VVP) formulation of system (3) is to find  $\mathbf{u} \in V^h$ ,  $\boldsymbol{\omega} \in \Sigma_v^h$ , and  $p \in Q^h$ , which minimize the functional

$$J_h(\mathbf{v}, \boldsymbol{\delta}, q) = \|\eta \nabla \times \boldsymbol{\delta} + \nabla q\|_0^2 + Kh^{-2} \|\nabla \cdot \mathbf{v}\|_0^2 + h^{-2} \|w_s(\nabla \times \mathbf{v} - \boldsymbol{\delta})\|_0^2, \quad (15)$$

over all  $\mathbf{v} \in V^h$ ,  $\boldsymbol{\delta} \in \Sigma_v^h$ , and  $q \in Q^h$ .

In both functionals (14) and (15),  $K$  is a positive constant, and the nonlinear weight  $w_s$  is defined in each element as

$$w_s(\mathbf{u}) = \frac{1}{\sqrt{1 + (G(\mathbf{u}))^2}}, \quad (16)$$

where  $G(\mathbf{u}) = \sqrt{2(\mathbf{D}(\mathbf{u}) : \mathbf{D}(\mathbf{u}))}$  is the shear rate. The double-dot product between two second-order tensors  $\boldsymbol{\tau}$  and  $\boldsymbol{\sigma}$  is defined as

$$\boldsymbol{\tau} : \boldsymbol{\sigma} = \sum_{i,j} \tau_{ij} \sigma_{ji}.$$

As stated for the Stokes problem in [4], results can be improved by sufficiently weighting the mass conservation term. Therefore, in our computations, we let  $K = 10^n$  and vary  $K$  from 0 to 8 to determine a proper  $K$  for convergent solution.



In fact, the resulted  $K$  for the two domains shown in Figure 1 are quite different. These will be reported and illustrated in our numerical results. Similar to the approach in [4], we solve the equations (14) and (15) iteratively with  $w_s(\mathbf{u})$  replaced by the previous iterate  $w_s(\mathbf{u}_0)$ . Here, we assume that the approximation

$$\mathbf{u}_0 \approx \mathbf{u}$$

satisfies  $\nabla \cdot \mathbf{u}_0 = 0$ , and

$$\max\{\|\mathbf{u}_0\|_\infty, \|\nabla \mathbf{u}_0\|_\infty\} \leq M < \infty. \quad (17)$$

Both functionals (14) and (15) were analyzed in [4] and [5]. This analysis suggested that using continuous piecewise linear elements for all variables, predicted discretization error bounds are  $O(h)$  in the  $L^2$ -norm for the approximations for  $\tau$ ,  $\omega$  and  $p$ , and  $O(h)$  in the  $H^1$ -norm for the approximation for  $\mathbf{u}$ . In contrast to those results, numerical results using the NWLS approach indicate that optimal convergence rates of  $O(h^2)$  can be expected for each component of the approximate solution of the Stokes equations, see [4], [5].

#### 4. Grading functions and adaptive algorithm for Stokes flow problems

In [10], a mesh redistribution algorithm in two spatial dimensions was developed by selecting two directions which can reflect the physics of the problems. Then, the one-dimensional equidistribution principle [9] is applied to the chosen directions. The one-dimensional grading function  $\xi(x)$ , defined in [9], has the property that after equidistribution, the inverse of  $\xi$  at  $i/N$ , where  $N$  is the number of elements in the domain, is the  $i^{\text{th}}$  grid point  $x_i$ . Let  $e = \phi - \phi_h$  and  $x_i$ ,  $i = 0, 1, 2, \dots, N$ , be the mesh of  $N$  intervals with  $h_i = x_i - x_{i-1}$  denoting the length of subinterval  $\Omega_i$ . The idea is to minimize the error of the interpolate in the  $H^m$ -seminorm, i.e., minimization of

$$|e|_m^2 = \int_a^b \left(e^{(m)}\right)^2 dx.$$

Based on this idea, the following grading function  $x_i$  was derived in [9]:

$$\xi(x) = \frac{\int_a^x (\phi'')^{2/[2(2-m)+1]} dx}{\int_a^b (\phi'')^{2/[2(2-m)+1]} dx}.$$

In [10], the one-dimensional grading function ( $m = 0$ ):

$$\xi = \frac{\int_a^x (\phi'')^{2/5} dx}{\int_a^b (\phi'')^{2/5} dx}, \quad (18)$$

which minimize the  $L^2$ -norm was considered.

In the following, we describe an adaptive algorithm to construct optimal grids of the least-squares approximations for our model equation (1). The procedures are essentially the same as those developed in [10] for the Galerkin finite element method. The algorithm in [10] is itemized in the following:

1. Select initial grids, e.g., quasi-uniform grids.
2. Triangulate the point set by an unstructured grid generation technique considered by Fortune [12]. After the triangulation, solve the problem by the finite element method.
3. Partition the given domain by a curve  $|\nabla\phi| = C$ , where  $u$  is the dependent variable problem and  $C$  is given by  $\left(\frac{\sum_{\Omega_i} |\nabla\phi|_{\Omega_i}^2 \cdot A_i}{A}\right)^{\frac{1}{2}} = C$ , where  $A_i$  is the area of the  $i^{th}$  element and  $A$  is the total area of the domain.
4. Choose the midpoint along the curve  $|\nabla\phi| = C$  to construct the flow line.
5. Specify the partitions  $M$  along the flow line, i.e.,  $M$  is the number of regions to be equidistributed. Once  $M$  is determined, equidistribute the point set  $\{s_i\}_{i=1}^{i=M-1}$  along the flow line according to the one-dimensional grading function.
6. Given the graded point set  $\{s_i\}_{i=1}^{i=M-1}$  obtained in the last step, construct the solution level curve  $\phi = \phi(s_i)$  for each  $i$ .
7. Determine the number of points  $N$  along each solution curve  $\phi = \phi(s_i)$  by  $N = \lceil \text{RATIO} \times M \rceil$ , where  $N$  is the greatest integer less than or equal to  $\text{RATIO} \times M$ , and  $\text{RATIO}$  is determined by  $\frac{(\sum \int |\nabla\phi|^2 ds)^{1/2}_{\phi=\phi(s_i)} \text{line}}{(\sum \int |\nabla\phi|^2 ds)^{1/2}_{\text{flow line}}}$ . This choice of  $N$  is essential for optimal rate of convergence.
8. Apply a one-dimensional grading function to equidistribute the solution level curve  $\phi = \phi(s_i)$  for each  $i$ . Since  $\phi$  is constant on each level curve, equidistribution results in uniform partitions. Therefore, uniform grids are used.
9. Determine the number of boundary nodes by the same method as in Step 7, and apply the grading function to equidistribute the boundary nodes.

10. Update the grid point information. Continue to Step 2 to triangulate the point set, check if the stopping criterion (the variation of the minimum  $h$  between consecutive iterations is less than some prescribed tolerance) is satisfied, and repeat the process if it's not.

In our computations, least-squares approximations and Delaunay triangulation procedures of Shewchuk [13] are used in Step 2. The above algorithm was modified in [14] for the transonic flow problem. It was reported that results can be greatly improved by extending the flow line to the boundary. Since incompressible flows are considered here, it is important to have sufficient inlet and outlet boundary points along the flow lines for the flow to be developed. Therefore, Step 9 is modified as follows:

- 9'. On the inlet and outlet boundaries, for example, on a unit square domain when  $x = 0.0$  and  $x = 1.0$ , the grid points are generated by extending the flow lines to these boundaries. On  $y = 0$  and  $y = 1.0$ , the  $x$ -coordinates of the grid points are the same as those nodes of the flow lines next to these boundaries. This principle will also applied to general domains, where the adaptive scheme is considered.

In addition, as illustrated in [11] and [15], Delaunay triangular meshes constructed in Step 2 are controlled such that the minimum degree of angles of the triangles is greater than 20 for quality meshes. In particular, for meshes used in the 4-to-1 contraction problem, all angles of the triangles are set to be between 25 and 130 degrees, and the maximum area of the triangles is set to be 0.0005 to avoid relatively huge grids. Finally, letting  $s$  be the arc length function along the flow line direction, the grading function

$$\xi(s) = \frac{\int_0^s g(t)dt}{\int_0^1 g(t)dt}, \quad (19)$$

where  $g = (\phi'')^{\frac{2}{5}}$  with  $\phi = |\mathbf{u}|_2$  for the square test domain and  $\phi = |\mathbf{u}|_1$  for the 4-to-1 contraction domain are used to illustrate the effectiveness and robustness of the algorithm.

## 5. Numerical results

In this section, two test problems are considered: the flow in the planar channel and in the 4-to-1 contraction problems. The symmetry of the geometry is used to reduce the computational domain by half, as shown in Figure 1. In our computations, continuous linear basis functions are considered for all variables.

### 5.1. Flow in the planar channel

The first problem is flow in a planar channel on the square domain  $[0, 1] \times [0, 1]$  considered in [16], where we have a line of symmetry along  $y = 0$ . The flow domain is shown in Figure 1(a). The exact solutions for  $(\mathbf{u}, p)$  in Cartesian coordinates are given in [16] by

$$\mathbf{u}_{exact} = \begin{bmatrix} 1 - y^4 \\ 0 \end{bmatrix}, \quad (20)$$

$$p_{exact} = -x^2. \quad (21)$$

Note that the exact solutions are obtained by adding the source terms,  $\mathbf{f}_1 = 0$ ,  $\mathbf{f}_2 = 0$ , and

$$\mathbf{f}_3 = \begin{bmatrix} 12y^2 - 2x \\ 0 \end{bmatrix}$$

in (2) and (3).

In our computations, the nonlinear weighted least-squares functionals (NWLS) are generated for two formulations of the Stokes equations: the VPS form (14) and VVP form (15). The coefficient  $K = 1$  related to mass conservation is considered first in these NWLS functionals. In addition, the viscosity is set to be  $\eta = 1$ . In the following, we demonstrate the capability of our algorithm in nonlinear weighted least-squares solutions for the Stokes equations.

To understand the influence of the initial meshes in our algorithm, two initial meshes in Figure 2 are considered: Mesh D, an  $8 \times 8$  uniform directional Delaunay triangular mesh; Mesh A, a controlled area Delaunay triangular mesh such that maximum triangle area is set to be 0.009.

Based on the VPS formulation (14), the nonlinear weighted least-squares method using the adaptive algorithm in Section 4 (called A-NWLS method) is performed using  $M = 8, 16$ , and 32 partitions along the chosen flow line. Following from the idea in [10], we use  $\phi = |\mathbf{u}|_2$  for this problem. As shown in Figure 3, similar convergent meshes are obtained from these initial meshes. Moreover, the  $L^2$  errors of graded mesh solutions using two initial Meshes D and A are plotted in Figure 4 and listed in Tables 1 and 2, respectively. Observe from Tables 1 and 2 that using initial Mesh D gives better results when the mesh is coarse. In the case of the finer mesh, similar results are obtained using initial Meshes D and A. Note that planar flow considered here is essentially a one dimensional flow. Since the solution curves  $u = C$  occur when  $y$  is constant, Mesh D is aligned along the solution curves  $u = C$ , and better results are expected.

From Table 3, observe that A-NWLS results only slightly improve the NWLS results using uniform Mesh D. As shown in Figure 4, the convergent mesh is coarse in the region when  $y \leq 0.5$ . This occurs because in this region,  $\nabla u$  varies slowly. Therefore, in Step 7 of the algorithm, the partition number  $N$  for the solution curves  $u \leq 0.5$  are relatively small compare to  $M$ . To maintain good quality of the grid, Delaunay triangular meshes constructed in Step 2 are controlled such that the minimum degree of angles of the triangles is greater than 20. We can also smooth the mesh using quasi-uniform grids in the coarse region  $y \leq 0.5$ . Therefore, Step 7 is modified as follows:

- 7'. In addition to Step 7, according to the  $N$  computed, order the solution curves  $\phi = \phi(s_i)$  in descending order, i.e.,  $\phi = \phi(s_1)$  has the largest partition number  $N$ . Set the partition number  $N$  for the solution curves  $\phi = \phi(s_i)$ ,  $i = M/2 - 1, \dots, M$ , to be the partition number for  $\phi = \phi(s_{M/2-1})$ .

The nonlinear weighted least-squares method based on this modified algorithm is called the H-NWLS method. Based on the VPS formulation (14), the H-NWLS methods using both initial meshes D and A are performed using  $M = 8, 16$ , and 32 partitions along the flow line. The convergent hybrid graded meshes are shown in Figure 5. As shown in Figure 5, similar convergent meshes are obtained from these initial meshes. Also, the  $L^2$  errors of hybrid graded mesh H-NWLS solutions using two initial meshes D and A are plotted in Figure 6 and listed in Tables 4 and 5, respectively. As illustrated in Figures 4 and 6, solutions of the H-NWLS method improve the rates of convergence over those of the A-NWLS in  $\mathbf{u}$ ,  $\tau$  and  $p$  from 1.8 to 2.4, 1.8 to 2.4, and 1.8 to 2.4, respectively, i.e., the optimal convergence rates can be restored using the H-NWLS method. The same observation applies to the VVP formulation (15), as illustrated in Tables 6 to 9.

To illustrate grid effects on convergence rates of least-squares solutions, two quasi-uniform meshes, Mesh D and Mesh A are considered. Also, two versions of least-squares solutions for (14) and (15) are considered: the NWLS method using quasi-uniform meshes and the H-NWLS method using quasi-uniform meshes as initial meshes in the hybrid adaptive algorithm. Using Mesh D, the  $L^2$  errors of these least-squares solutions are plotted in Figures 7 and 8 for the VPS and VVP formulations, respectively. Observed that the solutions of the H-NWLS method improve slightly over those of the NWLS for both formulations. However, from Figures 9 and 10, the  $L^2$  errors in the H-NWLS method are reduced more than those of NWLS method for both formulations using Mesh A. The results based on Figures 7 to 10 indicate that the grid effects on the NWLS solutions can be reduced

by the mesh redistribution algorithm, and the hybrid adaptive NWLS solutions are less sensitive to the initial meshes. Therefore, the adaptive algorithms are stable.

Note that from Tables 1, 2, 4, 5, and 6 to 9, we obtain similar  $L^2$  errors using similar numbers of elements for both formulations. However, the number of unknowns using the VPS formulation are 1.5 times more than those using the VVP formulation. In addition, as illustrated in these tables, the convergence rates of the A-NWLS solutions for the VVP formulation are optimal in  $\mathbf{u}$  and  $p$  while those for the VPS are suboptimal in  $\mathbf{u}$  and  $p$ . These results show that the mesh redistribution algorithms for the VVP formulation are more efficient than those for the VPS formulation.

Note that as stated for the Stokes problem in [4] and [5], optimal convergence rates of NWLS solutions were obtained using the mass conservation constant  $K = 100$ . In our numerical experiments, using  $K = 1$  in A-NWLS and H-NWLS methods is sufficient for optimal rates of convergence, which suggests that mass is conserved using optimal grid construction in the A-NWLS and H-NWLS approaches.

### 5.2. The 4-to-1 contraction problem

To illustrate further the capability of the NWLS schemes for the VPS and VVP forms, these methods are applied to the 4-to-1 contraction channel in Figure 1(b), with  $x$  (the flow direction) varying as  $-2 \leq x \leq 2$  and the contraction occurring at  $x = 0$ . The upstream channel width is 1, so the downstream width is  $1/4$ . The boundary conditions and  $\eta = 1.01$  are taken from those given in [6]. In [6], it was indicated that without the stabilized terms in the reduced GLS method, some oscillations occurred on the locally refined meshes around the corner. Therefore, comparing to results obtained in [6], systematic mesh refinements around the corner will be necessary. The details of the meshes considered are given in Table 10. They will be described subsequently. We start with a uniform criss-cross Mesh X in Figure 11 which is generated by Delaunay triangular grids with 8 partitions per unit length. Mesh X1 is obtained by refinement of Mesh X on  $[-1, 1]$ , and Mesh X2 refines Mesh X1 further on  $[-0.5, 0.5]$  as illustrated in Figure 12. Note that directional grids are considered on  $[-2, -1]$  here for efficiency. Similar types of mesh refinement were considered in [6].

Based on the work in [4] and [5], proper weight  $K$  must be chosen in the functionals (14) and (15) for optimal results. To illustrate the importance of the conservation constant  $K$ , the VPS form solution  $u$  at  $x = 0$  of the NWLS method using Mesh X2 using  $K = 1$ ,  $K = 100$ , and  $K = 1000$  are plotted in Figure 13.

Observe from Figure 13 that when  $K > 100$ , using the VPS formulation and Mesh X2, the NWLS solutions  $u$  at  $x = 0$  are similar and agree well with those of  $K = 100$ . Therefore,  $K = 100$  is sufficient to give satisfactory results. Similar results are obtained using the VVP formulation.

To compare results of the NWLS method using VPS and VVP formulations, the vertical velocity profiles on the axis of  $y = 0.25$  based on (14) and (15) of Meshes X, X1 and X2 are plotted in Figure 14. Figure 14 illustrates that convergent profiles are obtained for both VPS and VVP formulations. Note that the results of the VPS form compare well to those of [6] in the framework of the reduced GLS method using stabilized terms. In addition, these results are much better than those obtained by the reduced GLS solutions considered in [6] without the stabilized terms. However, as illustrated in Figure 14, slightly more oscillations occurred around the corner using the VVP formulation. As for the grid effects in the NWLS method reported in [11], Figure 14 shows that a refined regular mesh like Mesh X does not lead to instability and no grid effects are observed. Based on the above, using Meshes X1 and X2 type refinements of Mesh X near the corner of singularity, the NWLS results of the VPS formulation give better velocity profiles than those of VVP formulation.

In [17], for the VPS form, the authors reported that smooth results were obtained using the regular mesh and oscillatory solutions were observed using nonuniform mesh. To study the grid effects, we consider the second types of regular meshes Meshes UD1 and UD2 generated by selecting uniform Delaunay triangulation with 32 and 52 partitions per unit length, respectively. They are illustrated in Figure 15. Using Meshes X, UD1 and UD2, the profiles of the vertical velocity on the axis of  $y = 0.25$  for both VPS and VVP formulations of the Stokes problem are plotted in Figure 16. From Figure 16, observe that nonconvergence and instabilities profiles of the solution are obtained for both VPS and VVP forms. These results indicate that using linear approximations in all variables for the NWLS method will lead to instability of the solution with uniform Delaunay triangular grids. However, as illustrated in Figure 14, stable velocity profiles near the corner are observed using systematic mesh refinements of the regular criss-cross meshes in the NWLS method. Therefore, for both VPS and VVP forms, the oscillations are mesh dependent in the NWLS method. To reduce the influence of grid effects and resolve large flow variation near the corner, graded meshes generated by Delaunay triangulation will be investigated next.

Based on the success of the H-NWLS (NWLS based on the hybrid graded meshes) in the planar channel, the H-NWLS method is applied to a 4-to-1 con-

traction problem. The third set of meshes considered are the graded meshes generated by H-NWLS for both VPS and VVP forms using Mesh X as the initial mesh. They are shown in Figures 17 and 18. In order to better reflect the difference in the magnitude of two velocity components in this problem, here we use  $\phi = |\mathbf{u}|_1$  in the adaptive algorithm described in Section 4. Two graded meshes considered are described as follows: Mesh XH1, the hybrid graded mesh with regular grids on  $[-2, -1]$  and graded grids on  $[-1, 0.15]$  generated by the H-NWLS using  $M = 32$  partitions; Mesh XH2, the finer hybrid graded Mesh XH1 on  $[-1, 0.15]$  using  $M = 64$  partitions. Note that these graded meshes are more refined along the flow line on  $[-1, 0]$ . The profiles of the vertical velocity on the axis of  $y = 0.25$  are plotted in Figure 19. As illustrated in Figures 19(a) and 19(b), convergence profiles are obtained for both VPS and VVP formulations. Therefore, the instabilities of the solutions for both VPS and VVP forms can be reduced by increasing the partitions  $M$  along the flow line using graded mesh generated by H-NWLS.

In the following, we present results of VPS and VVP forms near the corner of singularity. Using NWLS with quasi-uniform Mesh X2 and adaptive Mesh XH2, velocity profiles of the vertical velocity on the axis of  $y = 0.25$  for both VPS and VVP forms of Stokes flows near the corner of singularity are plotted in Figure 20. From Figure 20(a), observe that the magnitude of the peak values of the VPS form are smaller than those of the VVP form. These results indicate that the inconsistency between the VPS and VVP formulations using NWLS with quasi-uniform Mesh X2. However, as illustrated in Figure 20(b), both forms give similar magnitude of the peak values using graded Mesh XH2. To investigate the inconsistency in the NWLS method further, we plot the minimum value  $v_{min}$  of the vertical velocity on the axis of  $y = 0.25$  against the number of unknowns in Figure 21. Note from Figure 21(a) that for the NWLS method, the values  $v_{min}$  of VPS are greater than those of VVP, but the difference in their values gets smaller as the number of unknowns increases. As for the H-NWLS method, from Figure 21(b), observe that when the number of unknowns is sufficiently large, the minimum value  $v_{min}$  of the vertical velocity on the  $y = 0.25$  of the H-NWLS method for VPS and VVP are in agreement. These results indicate that the H-NWLS method can reduce the grid effects of the NWLS method and therefore is more stable. In addition, as shown in Table 10, using the H-NWLS scheme, the number of elements can be reduced from 10120 (Mesh X2) to 7947 (Mesh XH2, VPS form) and 8261 (Mesh XH2, VVP form). Based on these results, for computational efficiency, it is sufficient to choose the hybrid graded mesh near



the corner of singularity. Results using Meshes XH1 and XH2 also indicate that stable and convergent results can be obtained by graded meshes refined along the flow line. Based on the above, when low-order basis functions are used, the grid effects in the NWLS method can be reduced by the H-NWLS scheme

The final set of meshes are the convergent graded meshes, which are obtained using a Union Jack grid Mesh J refined near the corner as an initial mesh. They are shown in Figure 22. Observe from Figures 17, 18 and 22 that similar convergent graded meshes of VPS and VVP are obtained using different initial meshes. Therefore, the adaptive algorithms are stable for the 4-to-1 contraction problem.

## 6. Conclusions

We have developed adaptive least-squares methods for solving VPS and VVP forms of the Stokes problems. The adaptive algorithm is stable because similar convergent adaptive graded meshes are generated using different initial meshes. For the planar flow problem, optimal convergence rates in all variables are obtained for both forms using the H-NWLS method. As for the 4-to-1 contraction problem, the graded meshes constructed are locally refined around flow lines which agree well with the physical attributes of the models. The grid effects in the NWLS method using lower-order basis functions in all variables can be reduced by the hybrid adaptive mesh which combines regular and graded grids. In addition, the inconsistency in the NWLS solutions between VPS and VVP forms can be resolved using the H-NWLS method. Also, in terms of the number of elements, graded meshes are more efficient than regular meshes. Finally, numerical experiments indicate that the H-NWLS method can be extended to more general 4-to-1 contraction problems without major difficulty.

## References

- [1] J.M. Kim, C. Kim, J. H. Kim, C. Chunga, K.H. Ahna, S. J. Lee, High-resolution finite element simulation of 4:1 planar contraction flow of viscoelastic fluid, *J. Non-Newtonian Fluid Mech.*, 129 (2005) 23-37.
- [2] T.F. Chen, C.L. Cox, H.C. Lee, K.L. Tung, Least-squares finite elements for generalized newtonian and viscoelastic flows, *Applied Numerical Mathematics* 60 (2010) 1024-1040.
- [3] P.B. Bochev, M.D. Gunzburger, Finite element methods of least-squares type, *SIAM, Review*, 40 (1998) 789-837.

- [4] H.C. Lee, T.F. Chen, A nonlinear weighted least-squares finite elements method for Stokes equations, *Computers and Mathematics with Applications*, 59 (2010) 215-224.
- [5] H.C. Lee, T.F. Chen, A nonlinear weighted least-squares finite elements method for velocity-vorticity-pressure formulation of Stokes equations, submitted (2011).
- [6] J. Bonvin, M. Picasso, R. Stenberg, GLS and EVSS methods for a three-field Stokes problem arising from viscoelastic flows, *Comput. Methods Appl. Mech. Engrg.*, 190 (2001) 3893-3914.
- [7] O.M. Coronado, D. Arora, M. Behr, M. Pasquali, Four-field Galerkin/least-squares formulation for viscoelastic fluids, *J. Non-Newtonian Fluid Mech.* 140 (2006) 132V144.
- [8] F. Zinani, S. Frey, Galerkin least-squares multifield approximations for flows of inelastic non-Newtonian fluids, *Journal of Fluids Engineering*, 130 (2008) 081507-1-081507-14.
- [9] G.F. Carey, H.T. Dinh, Grading functions and mesh redistribution, *SIAM J. Numer. Anal.*, 22 (1985) 1028-1040.
- [10] T.F. Chen, H.D. Yang, Numerical construction of optimal grids in two spatial dimensions, *Computers and Mathematics with Applications*, 39 (2000) 101-120.
- [11] H.C. Lee, Adaptive least-squares finite elements methods for viscoelastic flow problems, Ph.D. Thesis, Dept. of Mathematics, National Chung Cheng University, Taiwan, 2008.
- [12] S. Fortune, A sweepline algorithm for Voronoi diagrams, *Algorithmica* 2 (1987) 153-174.
- [13] J.R. Shewchuk, Triangle: engineering a 2D quality mesh generator and delaunay triangulator, in "Applied Computational Geometry: Towards Geometric Engineering" (Ming C. Lin and Dinesh Manocha, editors) , *Lecture Notes in Computer Science*, 1148 (1996) 203-222.
- [14] S.P. Chang, Optimal grids in the finite element approximations to compressible flow problem, Ph.D. Thesis, Dept. of Mathematics, National Chung Cheng University, Taiwan, 2006.

- [15] S.P. Chang, T.F. Chen, Optimal adaptive grids of least-squares finite element methods in two spatial dimensions, *Journal of Computational and Applied Mathematics*, (2011) doi:10.1016/j.cam.2011.01.028.
- [16] A. Fortin, R. Guenette, R. Pierre, On the discrete EVSS method, *Comput. Methods Appl. Mech. Engrg.*, 189 (2000) 121-139.
- [17] A. Fortin, M. Fortin, A new approach for the FEM simulation of viscoelastic flows, *J. Non-Newtonian Fluid Mech.*, 32 (1989) 295-310.

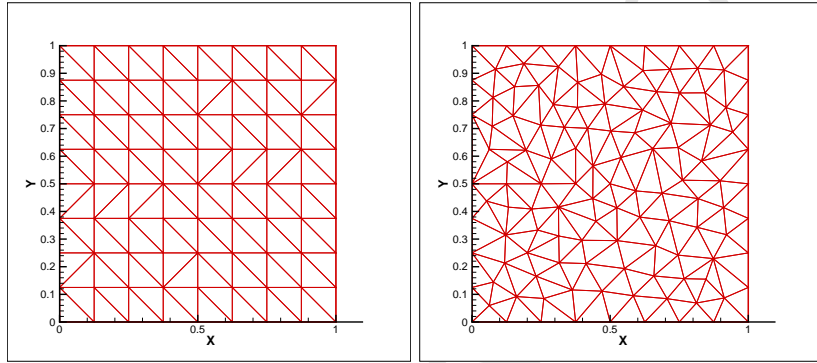


Figure 2: Initial meshes. Mesh D (left):  $8 \times 8$  uniform directional Delaunay triangular element, 128 elements. Mesh A (right): controlled area Delaunay triangulation, 174 elements.

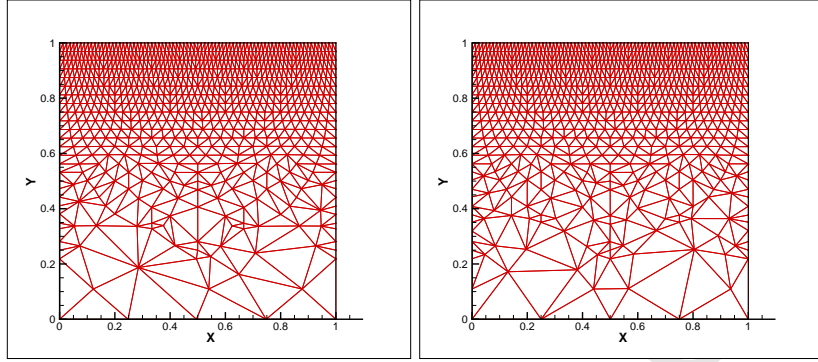


Figure 3: Convergent graded meshes using VPS form. 32 partitions along the flow line using initial meshes Mesh D (left, 5 iterations) and Mesh A (right, 5 iterations).

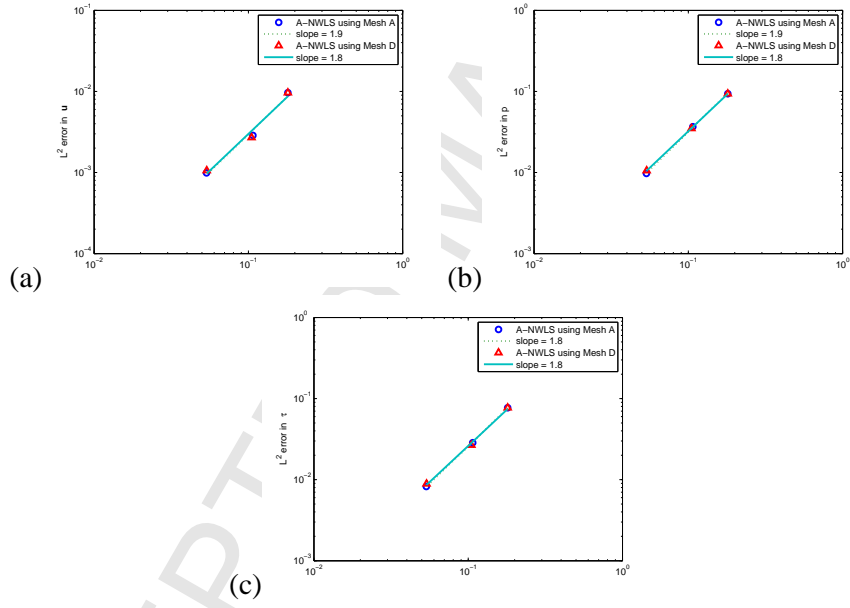


Figure 4: VPS form.  $L^2$  errors in A-NWLS solutions using initial meshes Mesh D( $\triangle$ ) and Mesh A(o).

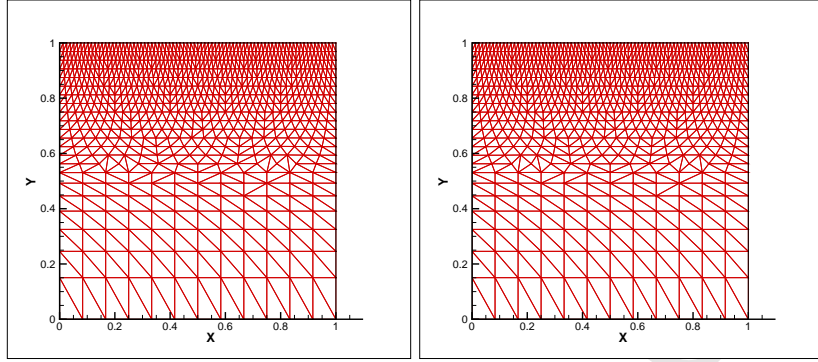


Figure 5: Hybrid convergent graded meshes using VPS form. 32 partitions along the flow line using initial meshes Mesh D (left, 5 iterations) and Mesh A (right, 5 iterations).

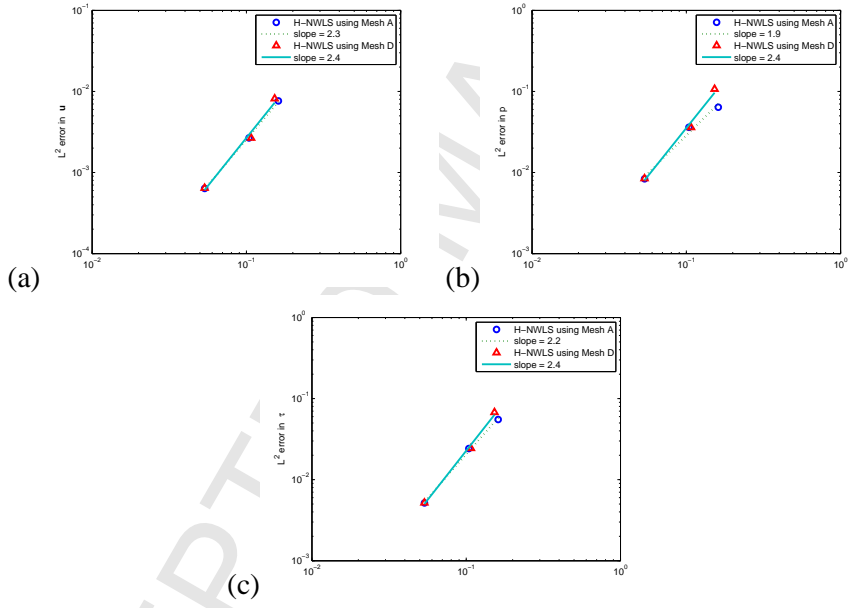


Figure 6: VPS form.  $L^2$  errors in H-NWLS solutions using initial meshes Mesh D( $\triangle$ ) and Mesh A( $\circ$ ).

Partitions	Elements	Unknowns	$h_{min}$	$\ \mathbf{u} - \mathbf{u}_{exact}\ _2$	$\ \boldsymbol{\tau} - \boldsymbol{\tau}_{exact}\ _2$	$\ p - p_{exact}\ _2$
8	123	408	0.069264	0.009652	0.077104	0.093732
16	364	1162	0.041835	0.002700	0.026689	0.034905
32	1386	4296	0.020037	0.001057	0.008877	0.010567

Table 1: VPS form.  $L^2$  errors in A-NWLS solutions using Mesh D as the initial mesh.

Partitions	Elements	Unknowns	$h_{min}$	$\ \mathbf{u} - \mathbf{u}_{exact}\ _2$	$\ \boldsymbol{\tau} - \boldsymbol{\tau}_{exact}\ _2$	$\ p - p_{exact}\ _2$
8	123	408	0.069264	0.009652	0.077104	0.093732
16	349	1116	0.041438	0.002871	0.028550	0.036726
32	1397	4330	0.020042	0.000990	0.008230	0.009732

Table 2: VPS form.  $L^2$  errors in A-NWLS solutions using Mesh A as the initial mesh.

Partitions	Elements	Unknowns	$h_{min}$	$\ \mathbf{u} - \mathbf{u}_{exact}\ _2$	$\ \boldsymbol{\tau} - \boldsymbol{\tau}_{exact}\ _2$	$\ p - p_{exact}\ _2$
$8 \times 8$	128	420	0.125	0.008612	0.083590	0.138063
$16 \times 16$	512	1604	0.0625	0.002187	0.021808	0.041457
$32 \times 32$	2048	6276	0.03125	0.000546	0.004599	0.009347

Table 3: VPS form.  $L^2$  errors in NWLS solutions using Mesh D as the initial mesh.

Partitions	Elements	Unknowns	$h_{min}$	$\ \mathbf{u} - \mathbf{u}_{exact}\ _2$	$\ \boldsymbol{\tau} - \boldsymbol{\tau}_{exact}\ _2$	$\ p - p_{exact}\ _2$
8	154	506	0.068711	0.007631	0.055165	0.063872
16	356	1138	0.041239	0.002667	0.024198	0.036121
32	1396	4326	0.020031	0.000636	0.005168	0.008359

Table 4: VPS form.  $L^2$  errors in H-NWLS solutions using Mesh D as the initial mesh.

Partitions	Elements	Unknowns	$h_{min}$	$\ \mathbf{u} - \mathbf{u}_{exact}\ _2$	$\ \boldsymbol{\tau} - \boldsymbol{\tau}_{exact}\ _2$	$\ p - p_{exact}\ _2$
8	128	420	0.125000	0.008149	0.067671	0.106806
16	351	1122	0.041766	0.002666	0.024330	0.035977
32	1396	4326	0.020030	0.000644	0.005190	0.008440

Table 5: VPS form.  $L^2$  errors in H-NWLS solutions using Mesh A as the initial mesh.

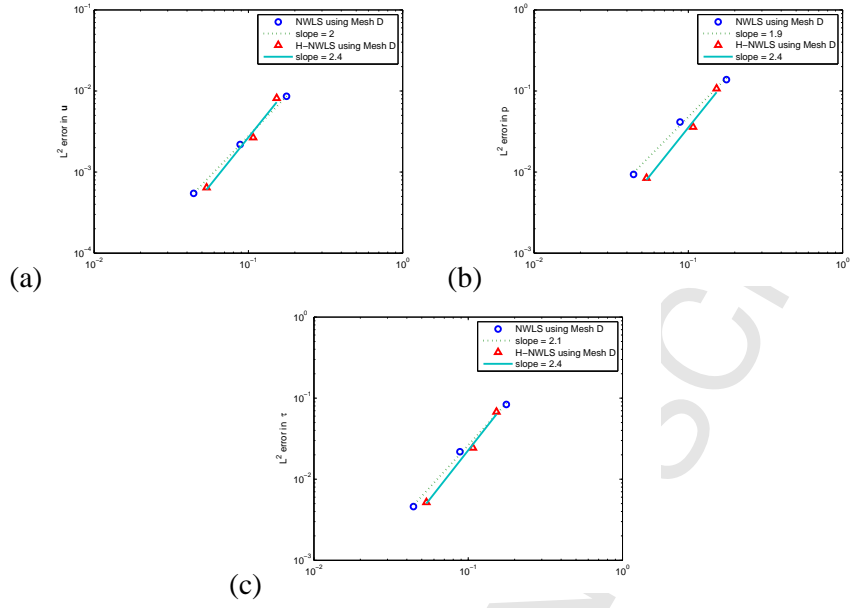


Figure 7: VPS form.  $L^2$  errors in (a)  $u$ , (b)  $p$  and (c)  $\tau$ . Results of NWLS using Mesh D(o) vs. H-NWLS( $\Delta$ ) using initial Mesh D.

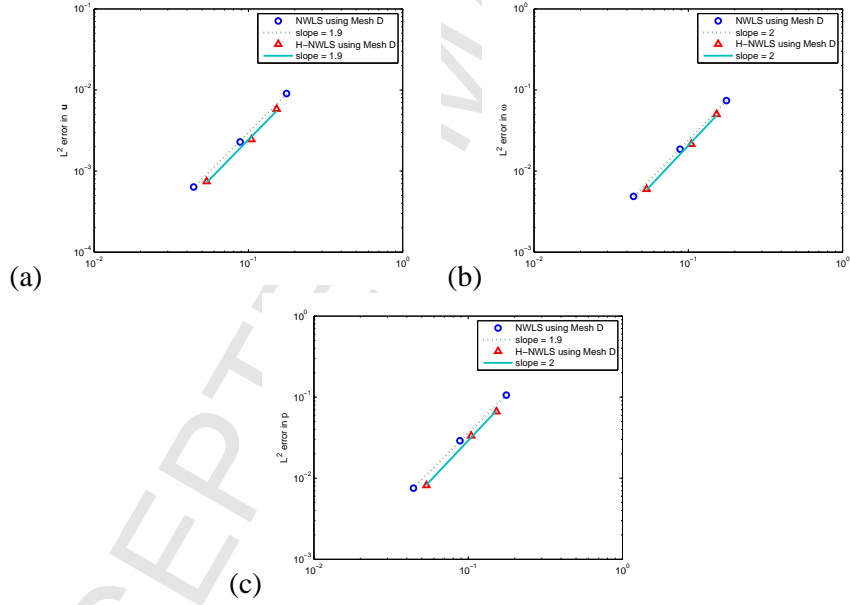


Figure 8: VVP form.  $L^2$  errors in (a)  $u$ , (b)  $\omega$  and (c)  $p$ . Results of NWLS using Mesh D(o) vs. H-NWLS( $\Delta$ ) using initial Mesh D.

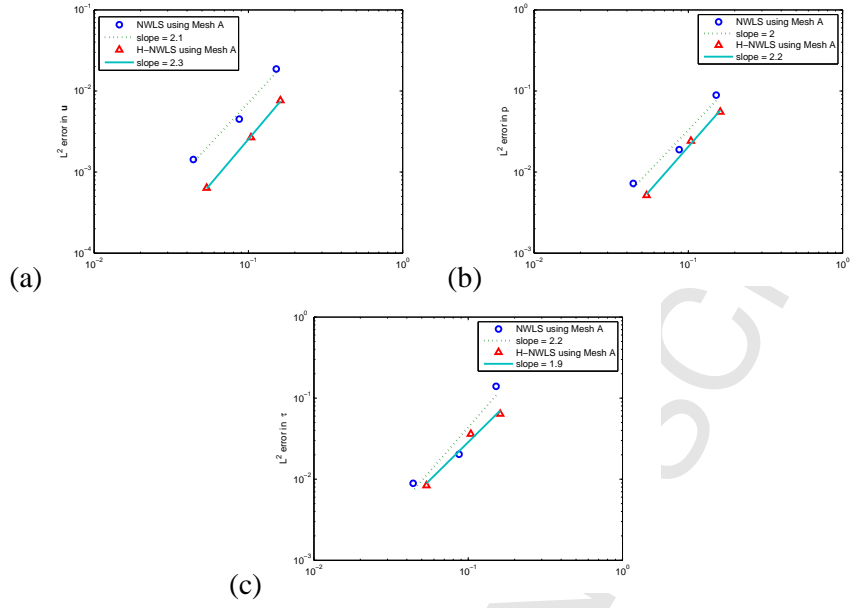


Figure 9: VPS form.  $L^2$  errors in (a)  $u$ , (b)  $p$  and (c)  $\tau$ . Results of NWLS using Mesh A(o) vs. H-NWLS( $\triangle$ ) using initial Mesh A.

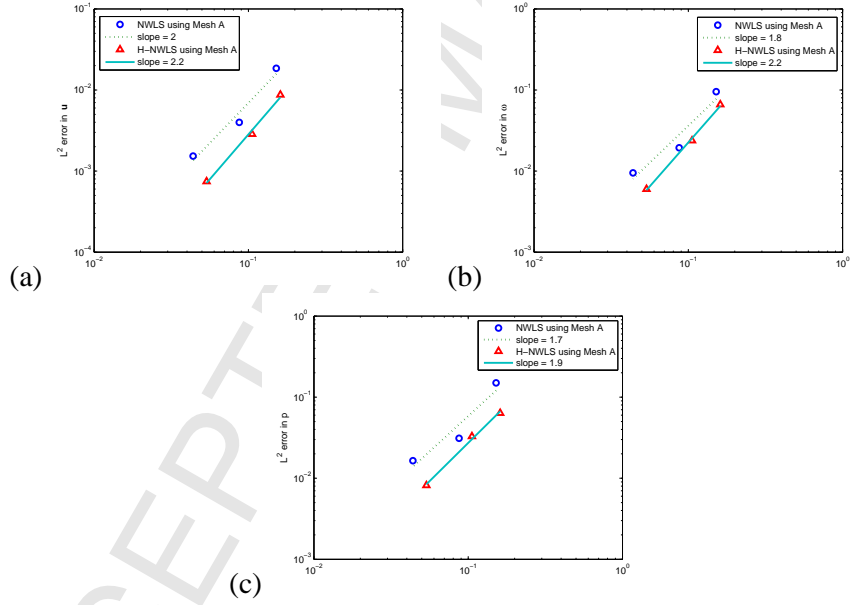


Figure 10: VVP form.  $L^2$  errors in (a)  $u$ , (b)  $\omega$  and (c)  $p$ . Results of NWLS using Mesh A(o) vs. H-NWLS( $\triangle$ ) using initial Mesh A.



Partitions	Elements	Unknowns	$h_{min}$	$\ \mathbf{u} - \mathbf{u}_{exact}\ _2$	$\ \boldsymbol{\omega} - \boldsymbol{\omega}_{exact}\ _2$	$\ p - p_{exact}\ _2$
8	115	231	0.068530	0.011444	0.104277	0.108737
16	350	701	0.042016	0.002850	0.039619	0.028141
32	1394	2789	0.020053	0.000823	0.008333	0.007041

Table 6: VVP form.  $L^2$  errors in A-NWLS solutions using Mesh A as the initial mesh.

Partitions	Elements	Unknowns	$h_{min}$	$\ \mathbf{u} - \mathbf{u}_{exact}\ _2$	$\ \boldsymbol{\omega} - \boldsymbol{\omega}_{exact}\ _2$	$\ p - p_{exact}\ _2$
8	127	255	0.067656	0.012454	0.117203	0.110289
16	361	723	0.041301	0.002856	0.038564	0.027301
32	1396	2793	0.020042	0.001006	0.007974	0.008081

Table 7: VVP form.  $L^2$  errors in A-NWLS solutions using Mesh D as the initial mesh.

Partitions	Elements	Unknowns	$h_{min}$	$\ \mathbf{u} - \mathbf{u}_{exact}\ _2$	$\ \boldsymbol{\omega} - \boldsymbol{\omega}_{exact}\ _2$	$\ p - p_{exact}\ _2$
8	172	345	0.068744	0.008721	0.063625	0.066181
16	365	731	0.041222	0.002857	0.032849	0.023737
32	1390	2781	0.020036	0.000745	0.008160	0.005989

Table 8: VVP form.  $L^2$  errors in H-NWLS solutions using Mesh A as the initial mesh.

Partitions	Elements	Unknowns	$h_{min}$	$\ \mathbf{u} - \mathbf{u}_{exact}\ _2$	$\ \boldsymbol{\omega} - \boldsymbol{\omega}_{exact}\ _2$	$\ p - p_{exact}\ _2$
8	154	309	0.068437	0.008590	0.063092	0.065417
16	355	711	0.041770	0.002906	0.032052	0.023557
32	1396	2793	0.020025	0.000743	0.008091	0.005924

Table 9: VVP form.  $L^2$  errors in H-NWLS solutions using Mesh D as the initial mesh.

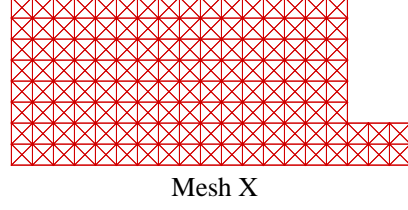


Figure 11: Uniform criss-cross mesh X with 8 partitions per unit length.

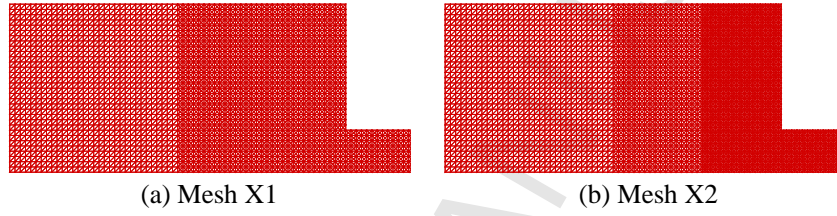


Figure 12: Systematic mesh refinements. (a) Mesh X1 with refinement on  $[-1, 1]$  of Mesh X and (b) Mesh X2 with refinement on  $[-0.5, 0.5]$  of Mesh X1.

Form	VPS	VPS	VVP	VVP
Mesh	Elements	Unknowns	Elements	Unknowns
X	640	1977	640	1282
X1	7680	23265	7680	10242
X2	10120	30669	10120	20242
UD1	3341	10211	3435	6508
UD2	6038	18373	6180	12362
XH1	5335	16233	5040	10082
XH2	7947	24185	8261	16524
J	640	1290	640	1977
JH	8139	24763	8883	17768

Table 10: Numbers of elements and unknowns for meshes using VVP and VPS forms in the 4-to-1 contraction problem.

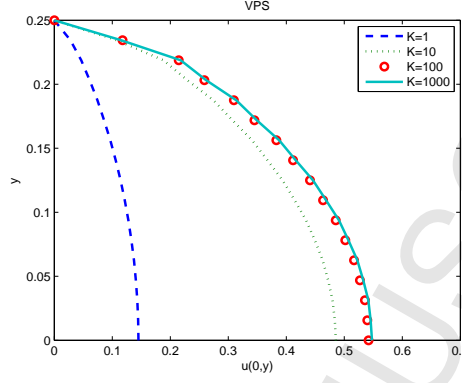


Figure 13: NWLS results of Mesh X2 for VPS form. Plots of  $u$  along the axis of  $x = 0$  for  $K = 1$ (- -),  $K = 10$ ( $\cdot\cdot$ ),  $K = 100$ ( $\circ$ ), and  $K = 1000$ (line).

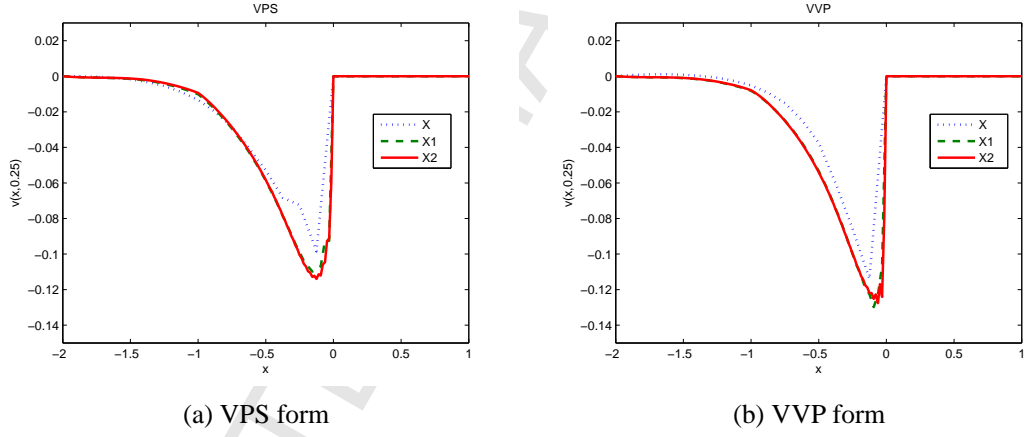


Figure 14: NWLS results of Mesh X ( $\cdot\cdot$ ), Mesh X1(- -) and Mesh X2(line). Plots of  $v$  along  $y = 0.25$  for (a) VPS and (b) VVP forms.

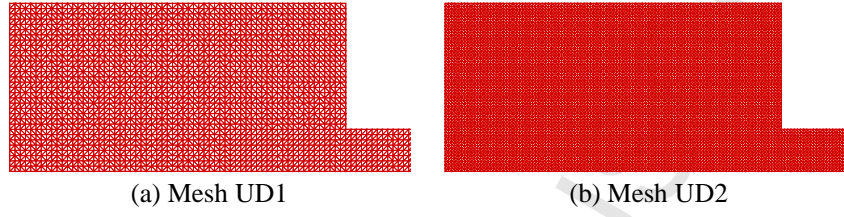


Figure 15: Refined uniform directional Delaunay triangular grids. (a) Mesh UD1 with 32 partitions per unit length and (b) Mesh UD2 with 52 partitions per unit length.

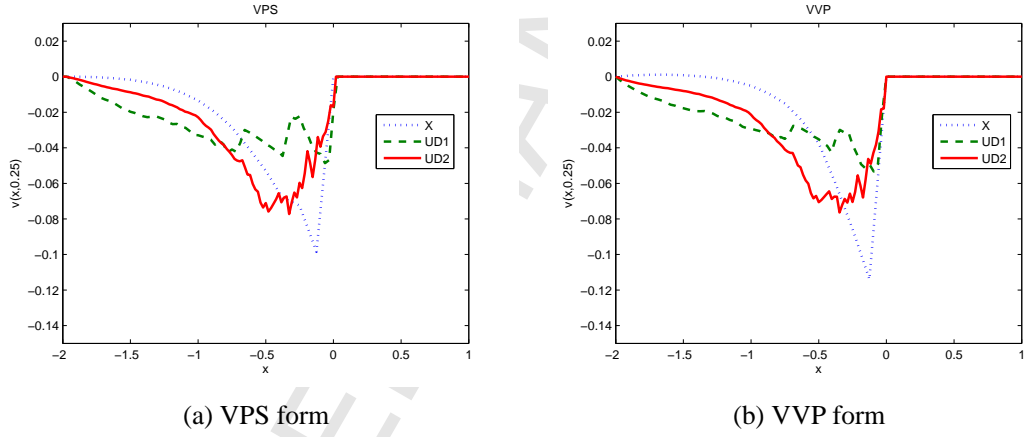


Figure 16: NWLS results of Mesh X(·) and Mesh UD1(-) and Mesh UD2(line). Plots of  $v$  along  $y = 0.25$  for (a) VPS and (b) VVP forms.

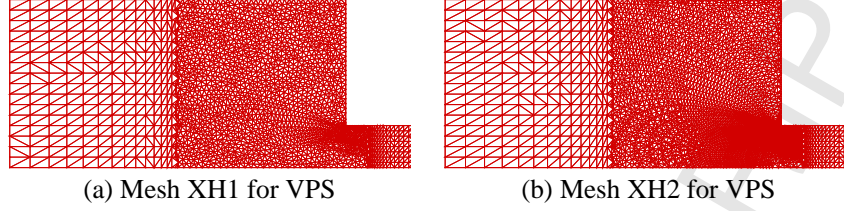


Figure 17: VPS form. Convergent graded meshes generated by H-NWLS method using initial Mesh X . (a) Mesh XH1 (32 partitions and 4 iterations). (b) Mesh XH2 (64 partitions and 3 iterations).

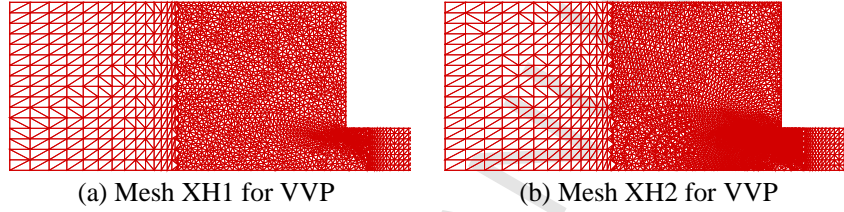


Figure 18: VVP form. Convergent graded meshes generated by H-NWLS method using the initial Mesh X . (a) Mesh XH1 (32 partitions and 4 iterations). (b) Mesh XH2 (64 partitions and 3 iterations).

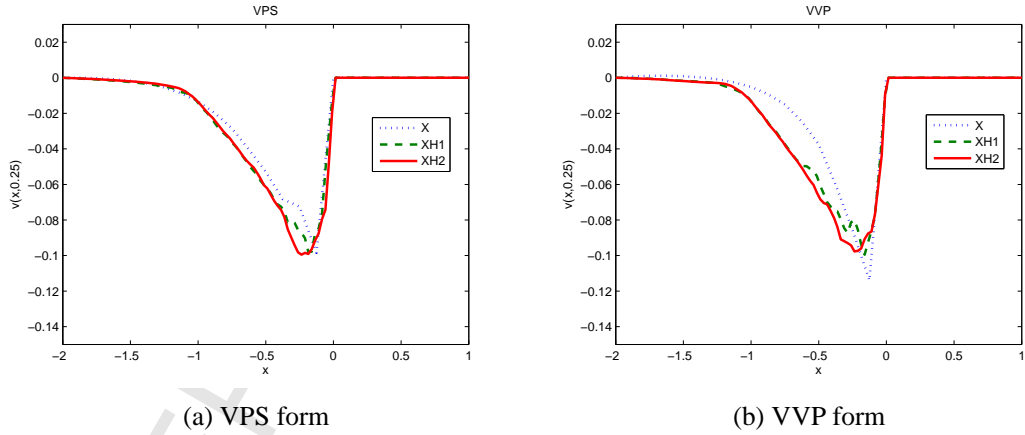
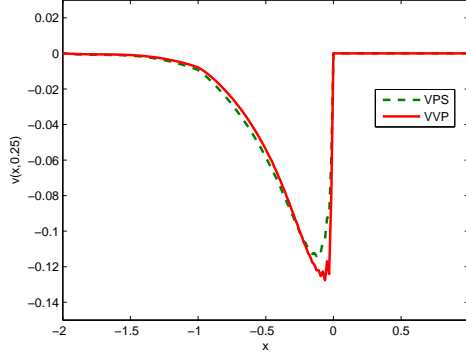
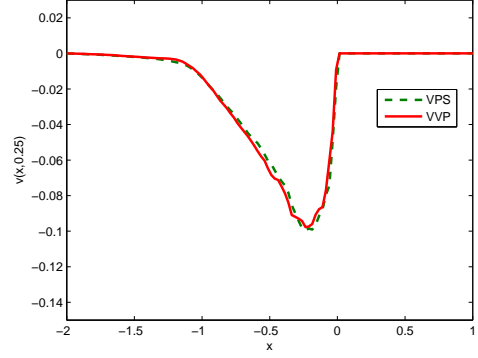


Figure 19: H-NWLS results of Mesh X(·) and Mesh XH1(- -) and Mesh XH2(line). Plots of  $v$  along  $y = 0.25$  for (a) VPS and (b) VVP forms.

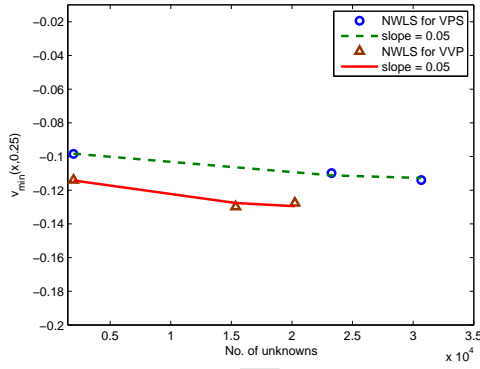


(a) NWLS results of Mesh X2

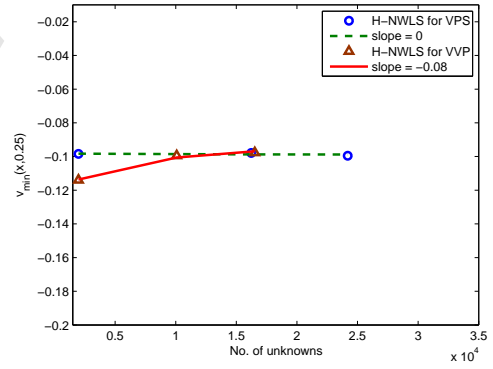


(b) H-NWLS results of Mesh XH2

Figure 20: Results of (a) NWLS method using regular mesh X2 and (b) H-NWLS method using hybrid graded mesh XH2. Plot of  $v$  along  $y = 0.25$  for VPS(- -) and VVP(line) forms.



(a) NWLS solutions



(b) H-NWLS solutions

Figure 21: Number of unknowns and  $v_{min}(x, 0.25)$  using VPS(o) and VVP( $\triangle$ ). (a) NWLS and (b) H-NWLS solutions.

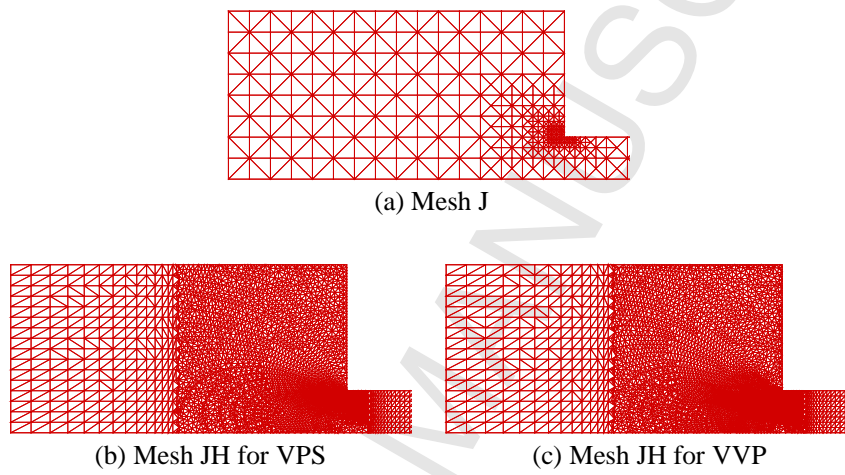


Figure 22: (a) Union Jack mesh J refined near the corner. (b) Mesh JH for VPS (64 partitions and 3 iterations): convergent graded mesh generated by H-NWLS method using initial Mesh J. (c) Mesh JH for VVP (64 partitions and 3 iterations): convergent graded meshes generated by H-NWLS method using initial Mesh J.

### Highlights

- Adaptive least-squares methods are used to solve the Stokes equations.
- Velocity-pressure-stress and velocity-vorticity-pressure formulations are used.
- Mesh redistribution for planar and 4-to-1 contraction flow problems are developed.
- Lower-order basis functions in all variables are used in least-squares methods.
- Hybrid meshes of regular and graded grids are used to reduce the grid effects .